I. J. Engineering and Manufacturing, **2025, 6, 1-15**
Published Online on December 8, 2025 by MECS Press (http://www.mecs-press.org/)
DOI: 10.5815/ijem.2025.06.01

Development of a Brain Tumour Detection and Classification Model with Web Application Capability

Kazeem B. Adedeji*
Department of Electrical and Electronics Engineering, Federal University of Technology Akure, Ondo State, Nigeria
E-mail: kbadedeji@futa.edu.ng
ORCID iD: https://orcid.org/0000-0002-2975-2965
*Corresponding Author

Obafunmilayo S. Lijadu
Department of Electrical and Electronics Engineering, Federal University of Technology Akure, Ondo State, Nigeria
E-mail: lijsamobafunmilayo@gmail.com

Wasiu Lawal
Department of Information and Communication Technology, Federal University of Technology Akure, Ondo State, Nigeria
E-mail: wlawal@futa.edu.ng
ORCID iD: https://orcid.org/0009-0005-9042-5831

Received: 11 November, 2024; Revised: 20 March, 2025; Accepted: 26 August, 2025; Published: 08 December, 2025

Abstract: In the evolving landscape of medical imaging, this study introduces a deep learning-based approach for brain tumour detection and classification. In this study, a U-Net architecture was developed for tumour detection and segmentation while an EfficientNet-based model was used for classification. Dataset consisting of MRI scans which has complex brain tumour pattern types was used to train the model. The performance of the developed model was evaluated using Dice coefficient, IoU score, sensitivity, and specificity for detection, and accuracy, precision, recall, and F1-score for classification, which demonstrates the system's effectiveness. The detection model achieves a Dice coefficient of 0.9321 and an IoU score of 0.8729, while the classification model attains an overall accuracy of 0.965, which surpasses the benchmark methods. Additionally, a user-friendly web interface was developed to enhance the system's practicality for clinical use. The results obtained show that the developed interface enables real-time tumour analysis. The proposed system not only improves the accuracy and efficiency of brain tumour analysis but also provides a seamless tool for medical professionals, which will enhance diagnostic workflows and patient outcomes.

Index Terms: Brain Tumour Detection, Deep Learning, U-Net, Efficientnet, MRI Analysis, Tumour Classification, Tumour Segmentation

1. Introduction

The human brain, as the central nervous system, governs critical functions such as cognition, communication, and emotional expression, enabling individuals to adapt to diverse environmental challenges [1]. However, this complex organ is susceptible to various diseases, one of the most prevalent and life-threatening ailment such as brain tumour. Brain tumour is abnormal cell growth that can be either primary (originating in the brain) or secondary (metastasizing from other parts of the body). These tumours range from benign (non-cancerous) (Fig. 1(a)) to malignant (cancerous) (Fig. 1(b)), with varying degrees of aggressiveness and severity. Symptoms such as headaches, seizures, blurred vision, and cognitive decline often depend on the tumour's size and location. Delayed or missed diagnoses can lead to permanent brain damage, neurological deficits, or even reduced life expectancy. Despite advancements in medical imaging, the healthcare system continues to face challenges in accurately detecting and diagnosing brain tumour. Traditional imagine modalities such as Magnetic Resonance Imaging (MRI) [2], Computed Tomography (CT) [3], Position Emission Tomography (PET) [4], and Magneto encephalography (MEGS) [5] have been widely used to identify brain abnormalities. Among these, the MRI stands out as the most effective due to its ability to provide high-

contrast images of brain tissues and structures [6].

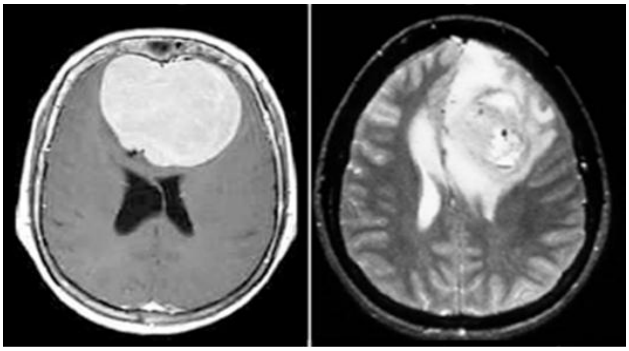

(a) (b)

Fig. 1. Brain tumour (a) benign (b) malignant.

In recent times, advances in human-computer interaction have led to the use of machine learning for brain tumor prediction. This paper focuses on leveraging advanced deep learning techniques to enhance the detection and classification of brain tumours using MRI data. By integrating U-Net for tumour segmentation and EfficientNet for classification, the proposed system aims to improve accuracy and efficiency in neuro-oncological diagnostics. The paper is organized as follows: Section 2 reviews related studies and outlines the contributions of this work. Section 3 details the methodology, including data preprocessing and model architecture. Section 4 presents the results and discussion, while Section 5 concludes the paper.

2. Review of Related Studies and Contribution

Several studies on deep learning-based brain tumour detection and classification systems have been published with varying degrees of success. In [7], a simplified CNN architecture was proposed for classifying three types of brain tumours: Glioma, Meningioma, and Pituitary. The model eliminates the need for region-based segmentation through direct classification using convolutional, max-pooling, and fully connected layers. When demonstrated on 3064 T1-weighted CE-MRI images, the system achieves a training accuracy of 98.51% and validation accuracy of 84.19%. Ari and Hanbay [8] presented a three-stage approach using an extreme learning machine with local receptive fields (ELM-LRF) for brain tumour classification. The system incorporates preprocessing for noise removal and combines ELM with local receptive fields for feature extraction. When tested on cranial MR images from 16 patients, the system achieves a classification accuracy of 97.18%, demonstrating superior performance compared to traditional CNN and Gabor wavelet approaches. Das *et al*. [9] introduced a CNN-based system with enhanced preprocessing, including Gaussian filtering and histogram equalization. The model was evaluated using 3064 T1-weighted contrast-enhanced MRI images from 233 patients. The system achieves a testing accuracy of 94.39%, showing significant improvement over existing methods. Deepak and Ameer [10] utilized transfer learning with GoogLeNet for feature extraction, combined with SVM and k-NN classifiers. When demonstrated on the public figshare dataset, the system achieves a classification accuracy of 98%, maintaining high performance even with reduced training samples.

Manjunath *et al*. [11] employed a combination of preprocessing techniques and CNN classification. The system utilizes Fuzzy C-Means clustering, GLCM, and LBP for feature extraction, followed by PCA for dimensionality reduction. The model achieves an accuracy of 86.49%, sensitivity of 72.97%, and specificity of 91.89% when tested on MRI scans. Sajid *et al*. [12] proposed a hybrid CNN architecture leveraging both local and contextual information. When evaluated on the BRATS 2013 dataset, the system demonstrates superior performance in segmenting core tumour regions and enhancing tumour areas. Ayadi *et al*. [13] developed a novel CNN model using 3 by 3 kernels with small stride values. The system was validated across three datasets: Figshare, Radiopaedia, and REMBRANDT, achieving accuracies of 94.74%, 93.71%, and consistent strong performance respectively. Çinar and Yildirim [14] presented a modified ResNet50 architecture with transfer learning. When tested on 253 images, the system achieves 97.2% accuracy, 94.7% sensitivity, and 100% specificity, outperforming established models like AlexNet and DenseNet201. Hashemzehi *et al*. [15] introduced a hybrid CNN-NADE model for improved distribution estimation. The system achieves 95% classification accuracy when tested on 3064 T1-weighted contrast-enhanced images using 6-fold cross-validation. Ismael *et al*. [16] proposed an enhanced ResNet-based model with data augmentation techniques. The system demonstrates state-of-the-art performance with 99% accuracy for image-level and 97% for patient-level classification. Saba *et al*. [17] presented a multi-step approach combining Grab cut segmentation with VGG-19 and handcrafted features. The system demonstrates high accuracy and DSC values across multiple BRATS datasets. Sharif *et al*. [18] developed a Saliency-based Deep Learning method with feature optimization using PSO. When evaluated on BRATS datasets, the system achieves dice similarity scores of 83.73% for core tumour and 93.7% for whole tumour

detection. Amin *et al.* [19] proposed a multi-step approach combining shape, texture, and intensity features with SVM classification. When demonstrated on Harvard, RIDER, and local datasets, the system achieves 97.1% accuracy, 0.98 AUC, 91.9% sensitivity, and 98.0% specificity. Sadad *et al.* [20] utilized a U-Net architecture with ResNet50 backbone and NASNet optimization. The system achieves the highest classification accuracy of 99.6% and an IoU score of 0.9504 when tested on 3,064 brain MRI slices.

Based on the examination of the existing literature, it is observed that while significant progress has been made in brain tumour detection and classification, there remains room for improvement in terms of model generalization and robustness across different datasets. While studies like Sadad *et al.* [20] achieve near-perfect accuracy, these results are often limited to specific datasets or conditions. This study aims to address these limitations by developing a more generalized approach that maintains high accuracy across diverse datasets and tumour types, while also reducing computational complexity and preprocessing requirements.

3. Methodology

The pipeline of the developed brain tumour detection and classification system is illustrated in Fig. 2. The system is designed to automate the analysis of brain MRI scans, providing accurate tumour detection and classification through a combination of deep learning models and a user-friendly web interface. The process begins with data collection, where MRI scans are gathered from publicly available datasets. These scans undergo preprocessing, which includes grayscale conversion, noise reduction, thresholding, contour detection, cropping, and data augmentation to enhance the quality and diversity of the input data. The preprocessed images are then fed into two distinct but complementary models:

(i) **Detection Model**: A U-Net architecture is employed for tumour detection and segmentation. This model is trained to identify tumour regions within the MRI scans, producing precise segmentation masks.

(ii) **Classification Model**: An EfficientNet-based model is used for tumour classification, categorizing the detected tumours into three types: meningioma, glioma, and pituitary.

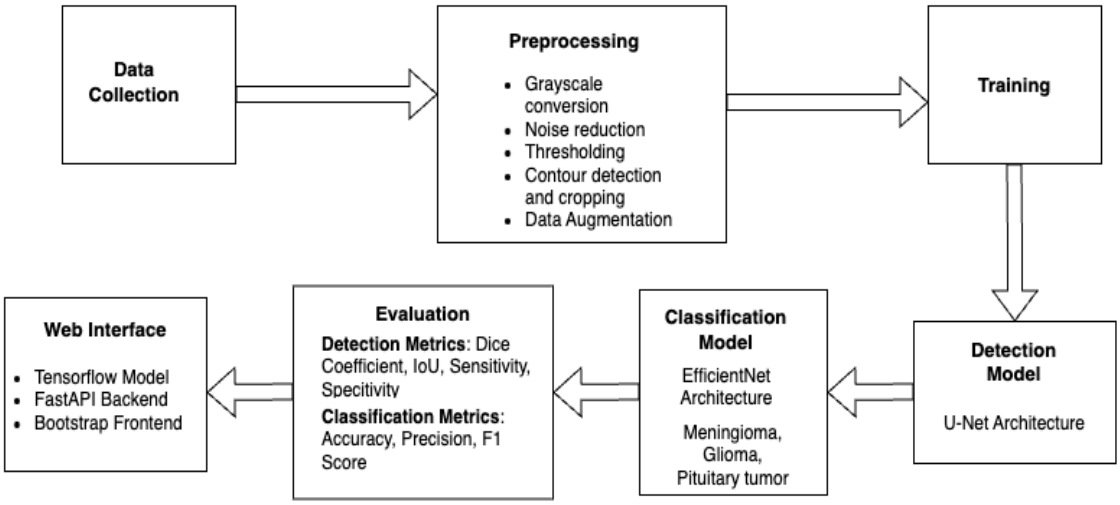

Fig. 2. Overview of deep learning based tumour analysis pipeline.

The performance of both models is rigorously evaluated using a range of metrics. For the detection model, metrics such as Dice coefficient, Intersection over Union (IoU), sensitivity, and specificity are used. For the classification model, accuracy, precision, recall, and F1-score are employed to assess performance.

3.1 Data Collection

The dataset used in this study was sourced from Kaggle, a widely recognized platform for machine learning datasets. It comprises a comprehensive collection of brain MRI images aggregated from multiple sources, including the Figshare dataset, the SARTAJ dataset, and the Br35H dataset. This combination provides a diverse set of MRI scans, essential for developing robust models for brain tumour classification. The dataset contains a total of 7,023 MRI images, categorized into four classes: glioma, meningioma, pituitary, and no tumour. The "no tumour" class images were obtained from the Br35H dataset, while the tumour classes (glioma, meningioma, and pituitary) were sourced from the Figshare and SARTAJ datasets.

Table 1 shows the distribution of the brain tumor class in the datasets. The class distribution in the dataset shows class imbalance. In this study, SMOTE was used to address class imbalance by generating synthetic samples for the minority class using the “fit-resample” method. This ensures an equal distribution of stroke and no-stroke instances. This distribution ensures that the model is trained to differentiate between healthy brain images and various types of

brain tumours, making it suitable for clinical applications. During the dataset preparation, an issue was identified with the glioma class in the SARTAJ dataset, where many images were incorrectly categorized. Given concerns about the accuracy of glioma classification in the SARTAJ dataset based on medical expert advice, to address this, the images were replaced with those from Figshare. This adjustment was necessary to maintain dataset integrity and ensure accurate model training. The diversity and size of the dataset make it ideal for tasks involving brain tumour detection and classification, providing a solid foundation for training and evaluating deep learning models.

Table 1. Data distribution in the selected dataset.

Brain tumor classes	Source Dataset	Number of images
Glioma	Figshare	1621
Meningioma	SARTAJ	937
	Figshare	708
Pituitary	Figshare	856
	SARTAJ	901
No tumor	Br35H	1500
	SARTAJ	500

3.2 Preprocessing

(a) Grayscale Conversion and Gaussian Blur

Each image is converted to grayscale using (1), which reduces the dimensionality of the data while retaining the crucial structural information needed for tumour classification.

$$I_{gr} = 0.299R + 0.587G + 0.114B \tag{1}$$

where I_{gr} is the converted grayscale image, R, G and B are the red, green, and blue pixel values, respectively. The result of this conversion is shown in Fig. 3(a), where the image has been transformed into a single-channel grayscale representation. A Gaussian blur of 5×5 kernel is applied to each grayscale image using (2). This operation helps to reduce noise and smooth out fine details that may not be relevant for tumour classification.

$$I_{blr} = \frac{1}{2\pi\sigma^2} e^{-\frac{x^2+y^2}{\sigma^2}} \tag{2}$$

where I_{blr} is the blurred image, x and y are the pixel coordinates, and σ is the standard deviation of the Gaussian distribution, controlling the level of blurring. The result of this process is shown in Fig. 3(b), where the image is smoothed, reducing high-frequency noise.

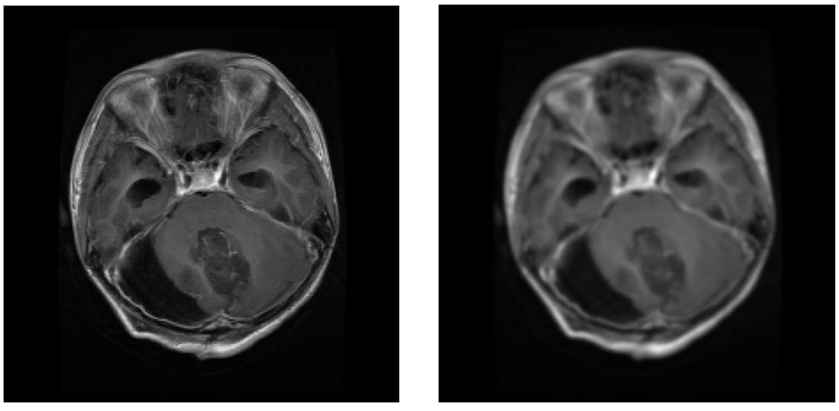

(a) (b)

Fig. 3. Preprocessing (a) grayscale image (b) gaussian blurred image.

(b) Thresholding and Morphological Operations

The blurred image is then given a threshold to create a binary image, which helps in segmenting the brain region from the background. This is achieved by applying a fixed threshold T, where pixel values greater than T are set to white (255), and those below are set to black (0) using (3).

$$I_{bn}(x,y)=\begin{cases}255 & if\ I_{blr}(x,y)>T\\ 0 & if\ I_{blr}(x,y)\le T\end{cases} \tag{3}$$

where I_{bn} is the threshold image. In this case, the threshold value of 45 was used. The result of the thresholding is shown in Fig. 4(a), where the brain region is clearly segmented from the background. Erosion and dilation operations are applied to the binary image, helping to remove small noise regions and fill in small holes within the segmented brain region. Erosion shrinks the white regions by removing pixels from the boundaries of objects. This is achieved using a structuring element as in (4), where each pixel is replaced by the minimum pixel value under the element.

$$I_{errd}(x,y)=\min\left[I_{bn}(x+u,y+v)\right] \tag{4}$$

where I_{errd} is the eroded image and u and v the coordinates within the structuring element. After erosion, dilation is applied using (5), which expands the white regions by adding pixels to the boundaries.

$$I_{dil}(x,y)=\max\left[I_{errd}(x+u,y+v)\right] \tag{5}$$

where I_{dil} the dilated image. These steps refine the segmentation by reducing noise and closing small gaps in the brain region. The result is shown in Fig. 4(b), where the brain area appears cleaner and more distinct.

(a) (b)

Fig. 4. (a) thresholded image (b) image after erosion and dilation.

(c) Contour Detection, Region of Interest (ROI) Extraction and Resizing

Contours are detected in the processed binary image as shown in Fig. 5(a). The largest contour, presumably corresponding to the brain region, is identified. The extreme points (left, right, top, bottom) of the largest contour, shown in Fig. 5(b) are used to define a bounding box around the brain region. The original image is then cropped to this region, effectively removing irrelevant background information. Finally, the cropped image is resized to 224×224 pixels with cubic interpolation as shown in Fig. 5(c). This ensures that all input images have consistent dimensions as required by the EfficientNet model.

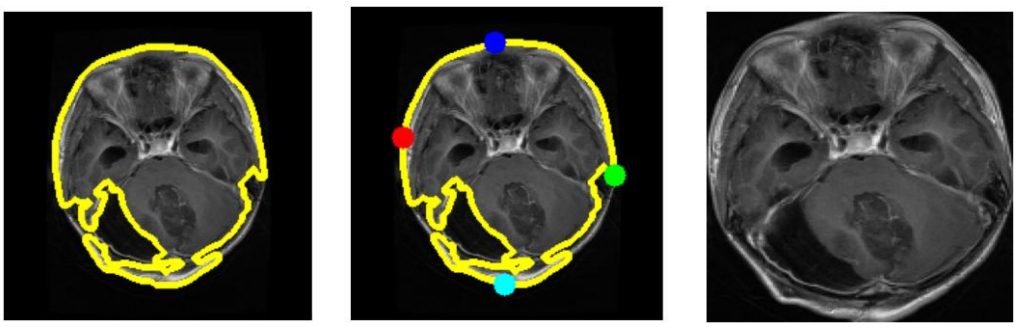

(a) (b) (c)

Fig. 5. (a) image with contour (b) image with extreme points (c) cropped image.

3.3. Training and Optimization

3.3.1 Tumor Detection: U-Net Architecture

For tumour detection and segmentation, a U-Net architecture was employed due to its proven effectiveness in medical image analysis [21, 22]. U-Net and EfficientNet excel over other advanced alternatives like Vision Transformers (ViTs) in medical image segmentation tasks because they exhibit better computational efficiency, and has superior handling of local image details through its convolutional architecture and skip connections [21, 22]. The U-Net model consists of an encoder path, a bridge, and a decoder path. The encoder path includes three convolutional blocks, each containing two 3x3 convolutional layers followed by a ReLU activation function and a 2x2 max-pooling layer. The number of filters doubles in each block, starting from 64 and increasing to 256, enabling the extraction of increasingly abstract features. The bridge section processes the encoded features using two 3x3 convolutional layers with ReLU activation and 512 filters. The decoder path mirrors the encoder, with three upsampling blocks that restore the original spatial resolution. Each block includes an upsampling operation, a 2x2 convolutional layer, and skip connections to integrate features from the encoder. The final layer consists of a 1x1 convolution with a sigmoid activation function, followed by Global Average Pooling, producing a binary classification output. The model accepts 256x256 RGB images and is optimized using the Adam optimizer with a binary cross-entropy loss function. The hyperparameters used for the U-Net model are listed in Table 2. Data augmentation techniques, including random flips, rotations, zoom adjustments, and brightness variations, were applied to enhance robustness and generalizability. Regularization techniques such as L2 regularization and dropout were implemented to prevent over fitting. A ReduceLROnPlateau scheduler dynamically adjusted the learning rate, and early stopping was applied if no improvement was observed.

Table 2. U-Net detection model hyperparameters.

Parameters	**Values**
Number of Epochs	20(maximum)
Batch Size	32
Initial Learning Rate	$1e^{-4}$
Optimizer	Adam
Loss Function	Binary Cross-Entropy
L2 Regularization Factor	$1e^{-5}$
Dropout Rate	0.3
Learning Rate Scheduler	ReduceLROnPlateau (factor: 0.1, patience: 5 epochs)
Early Stopping Patience	10 epochs

3.3.2 Tumor Classification: EfficientNet-based Architecture

For tumour classification, an EfficientNetV2B0 model was utilized, leveraging its compound scaling method for efficient and effective feature extraction. The base model, pre-trained on ImageNet, was adapted by modifying its top layers. A global average pooling layer was followed by a dense layer with 256 units and ReLU activation, a dropout layer with a rate of 0.5, and a final dense layer with softmax activation for multi-class classification. The hyperparameters used for the EfficientNet-based classification model are listed in Table 3. Training was conducted over a maximum of 50 epochs, using a batch size of 32. The Adam optimizer was employed with an initial learning rate of $1e^{-3}$, coupled with an exponential decay schedule. The training process was divided into two phases: the first 10 epochs with frozen base model weights, followed by fine-tuning the top 30 layers. Class weights were applied to address dataset imbalance, ensuring equal consideration for all classes. Training for both models was conducted on Google Colab's A100 GPU using TensorFlow 2.17.0 and Keras.

Table 3. EfficientNet classification model hyperparameters.

Parameters	**Values**
Number of Epochs	50 (maximum)
Batch Size	32
Initial Learning Rate	$1e^{-3}$
Optimizer	Adam
Loss Function	Categorical Cross-Entropy
Learning Rate Decay	Exponential (factor: 0.9 every 10,000 steps)
Dropout Rate	0.5 (before final dense layer)
Early Stopping Patience	10 epochs

3.4 Web Interface Development

To translate the research findings into a practical tool for medical professionals, a user-friendly web interface as illustrated in Fig. 6 was developed to facilitate the seamless integration of the brain tumour detection and classification models into clinical workflows. This interface will provide an intuitive and accessible platform for uploading MRI scans, processing the images through the trained models, and visualising the results.

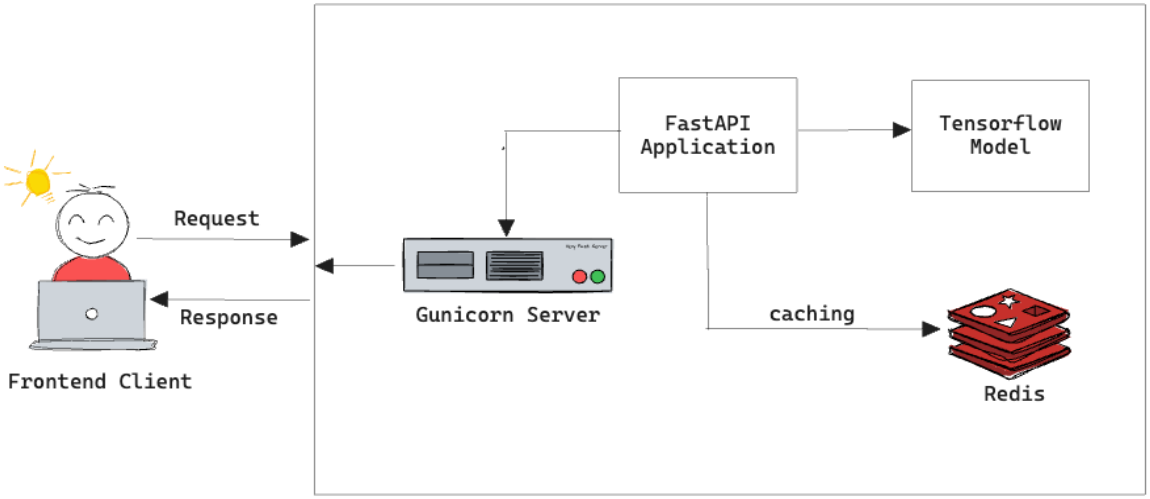

Fig. 6. Overview of the web interface.

The web interface incorporated the following key features:

(i) **Image Upload:** Users will be able to upload MRI images in various formats, including JPEG, JPG, and PNG.
(ii) **Image Preprocessing:** Upon upload, the images will undergo automated preprocessing using the established pipeline described earlier.
(iii) **tumour Detection and Classification:** The uploaded image will first be analysed by the trained U-Net model to detect the presence of a tumour. If a tumour is identified, the image will then be passed to the EfficientNet classifier for tumour type determination. If no tumour is detected, the process will stop after the detection step.
(iv) **Result Visualisation:** The web interface will present the original image along with the analysis results. If a tumour is detected, the classification result (tumour type) will be displayed along with associated confidence scores.

3.5 Performance Evaluation

The performance of the developed model was assessed based on some metrics used for brain tumor analysis. These metrics are categorized as under tumor detection and classification metrics.

3.5.1 Tumour Detection Metrics

For the tumour detection task, the following metrics were used:

(a) Dice coefficient: This metric quantifies the overlap between predicted tumour regions and ground truth segmentations. It provides a sensitive measure of spatial accuracy. The Dice coefficient D was estimated using (6)

$$D = \frac{\left(2 \times |X \cap Y|\right)}{\left(|X| + |Y|\right)} \tag{6}$$

where X the predicted segmentation and Y is the ground truth segmentation.

(b) Intersection over Union (IoU): The IoU score offers an alternative perspective on segmentation accuracy by measuring the overlap relative to the combined area of predicted and actual tumour regions. This was estimated using (7).

$$IoU = \frac{|X \cap Y|}{|X \cup Y|} \tag{7}$$

(c) Sensitivity (True Positive Rate): This measures the model's ability to correctly identify tumour regions and was estimated using

$$SS = \frac{TP}{TP + FN} \tag{8}$$

where *SS* is the sensitivity, *TP* is the positives and *FN* is the false negatives.

(d) Specificity (True Negative Rate): This measures the model's ability to correctly identify non-tumour regions and is estimated using

$$SP = \frac{TN}{TN + FP} \tag{9}$$

where *SP* is the specificity, *TN* is the true negatives and *FP* is the false positives.

3.5.2 Tumour Classification Metrics

For the tumour classification task, metrics suited to multi-class classification problems was utilized. These metrics helps to evaluate how well the EfficientNet-based model distinguishes between different tumour types and healthy brain tissue. The following metrics were used:

(i) Accuracy: This measures the overall proportion of correct classifications across all classes. The accuracy *A* was estimated using

$$A = \frac{TP + TN}{TP + TN + FP + FN} \tag{10}$$

(ii) Precision: This quantifies the model's ability to avoid false positives for each class. The precision *P* was estimated using (11).

$$P = \frac{TP}{TP + FP} \tag{11}$$

(iii) Recall: This measures the model's capacity to identify all instances of a particular tumour type and is estimated using Eq. (8).

(iv) F1-score: This provides a balanced measure of performance, considering both precision and recall. This was estimated using (12).

$$P = 2 \times \frac{P \times R}{P + R} \tag{12}$$

(v) ROC (Receiver Operating Characteristic) Curve: This evaluates the model's ability to distinguish each tumour type from the others. The curves help visualise the trade-off between sensitivity and specificity for each tumour type.

In addition to these specific metrics, the confusion matrices for both tasks were also generated to provide visual insights into the models' strengths and weaknesses. For the detection model, the confusion matrix illustrated the true positive, true negative, false positive, and false negative rates at the pixel level. For the classification model, it provided a detailed breakdown of predictions across all classes, allowing us to identify any consistent misclassifications.

4. Results and Discussions

4.1. Detection Model Results

The training and validation performance of the U-Net based detection model over 20 epochs is illustrated in Fig. 7. As shown in Fig. 7(a), the training loss consistently decreases, indicating the model's capacity to effectively learn the task. In contrast, the validation loss shows minor fluctuations but generally follows a downward trend, suggesting that the model's generalisation improves over time with the validation set, though some noise is present in the validation process. The accuracy curve (Fig. 7(b)) similarly shows strong performance, with training accuracy steadily increasing. Validation accuracy exhibits more variability, reflecting potential fluctuations in the model's ability to generalise.

Despite this variability, validation accuracy remains relatively close to the training accuracy, indicating no significant overfitting.

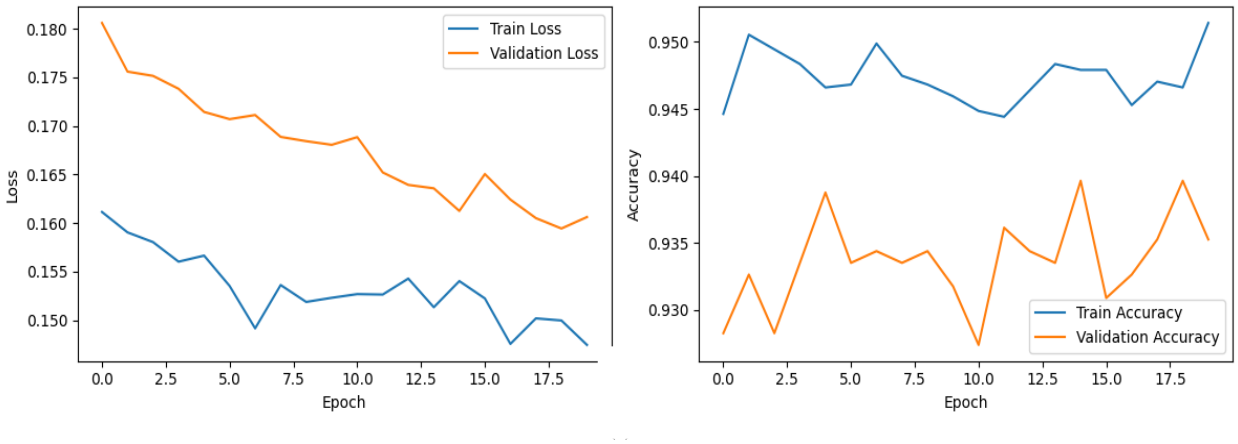

(a) (b)

Fig. 7. Training and validation performance curves for detection model (a) model loss (b) model accuracy.

After training, the model was tested on the test dataset, yielding impressive results in segmenting tumour regions from MRI scans. The results are shown in Table 4. These scores indicate strong overall performance, but the confusion matrix in Fig. 8 provides a more nuanced view of the model's capabilities. The matrix shows 359 true negatives cases where the model correctly identified non-tumour regions, and 831 true positives where it accurately detected tumour regions. These high numbers of correct classifications align with the impressive sensitivity and specificity scores. The model also produced 46 false positives instances where it incorrectly identified non-tumour regions as tumours, and 75 false negatives cases where it failed to identify existing tumours. These results closely mirror the calculated sensitivity and specificity. The model demonstrates a robust ability to correctly identify both tumour and non-tumour regions, with a slight bias towards tumour detection. This bias is generally preferable in medical diagnostics, where missing a tumour (false negative) is typically more concerning than a false alarm (false positive).

Table 4. Detection model evaluation metrics.

Metric	Score
Dice Coefficient	0.9321
IoU Score	0.8729
Sensitivity	0.9172
Specificity	0.8864

The high number of true positives (831) compared to false negatives (75) confirms the model's high sensitivity (0.9172). This characteristic is crucial in a clinical context, as it indicates the model rarely misses existing tumour, which is vital for early detection and intervention. Similarly, the model's specificity (0.8864) is reflected in the

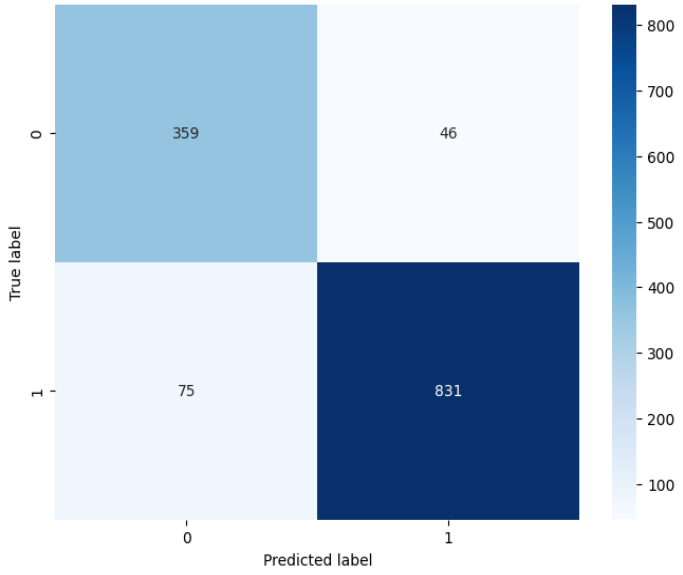

Fig. 8. Confusion matrix of the detection model.

relatively high number of true negatives (359) compared to false positives (46). This suggests that while the model is very good at identifying healthy tissue, it has a slight tendency to over-predict tumour. Particularly, a small number of false positives (46) were observed. This indicates that when the model identifies a tumour, it is highly likely to be correct. Such performance could potentially reduce unnecessary follow-up procedures or patient anxiety from false alarms. The slightly higher number of false negatives (75) compared to false positives suggests there's room for improvement in the model's ability to detect all tumour instances. However, given the overall high performance, these may represent particularly challenging cases that could benefit from expert review.

4.2. Classification Model Results

The training and validation performance curves shown in Fig. 8 indicate that the model effectively learns over time, with training loss (Fig. 9(a)) steadily decreases and accuracy (Fig. 9(b)) improving, reaching around 90% by the final epoch. Although validation loss fluctuates in the early and mid-training stages, it stabilises toward the end, suggesting that the model generalises well to unseen data. The validation accuracy closely tracks the training accuracy, albeit with some fluctuations, indicating minor overfitting. Despite these variations, the model demonstrates strong overall performance, suggesting that it effectively balances learning and generalisation.

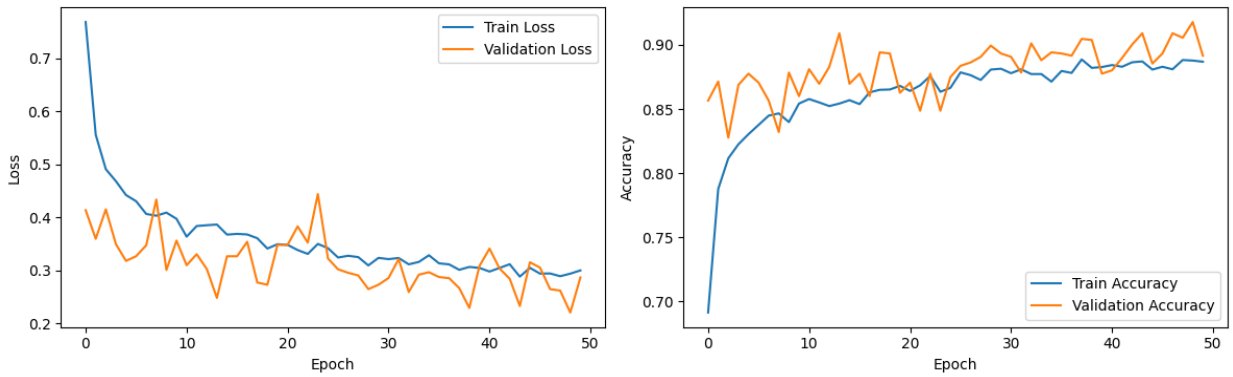

(a) (b)

Fig. 9. Training and validation performance for the classification model (a) model loss (b) model accuracy.

After training, the classification model was evaluated on the test dataset, yielding impressive results in accurately classifying tumour types from MRI scans. The results are shown in Table 5.

Table 5. Classification model evaluation metrics

Class	Precision	Recall	F1-score	Support
Pituitary	0.80	0.99	0.89	300
Glioma	0.89	0.81	0.85	300
Meningioma	0.81	0.71	0.76	306
No tumour	0.98	0.97	0.97	405

Fig. 10 shows the confusion matrix of the classification model. This provides valuable insights into the model's classification performance across the four categories: Pituitary (0), Glioma (1), Meningioma (2), and No tumour (3). For the "No tumour" class, the model demonstrates excellent performance, correctly identifying 391 out of 405 cases. This high accuracy (96.5%) suggests the model could be a valuable screening tool, potentially reducing radiologists' workload by reliably identifying healthy brain scans. The few misclassifications (9 as Meningioma, 5 as Glioma) indicate very low false positive rates for tumours. The model's performance on Pituitary tumours is outstanding, with 296 correct classifications out of 300 cases. This 98.7% recall rate shows the model excels at identifying this specific tumour type. Only 4 cases were misclassified as Glioma, indicating minimal confusion with other tumour types. For Gliomas, the model correctly identified 243 out of 300 cases (81% recall). While this represents good performance, there's room for improvement. The model occasionally misclassified gliomas as meningiomas (43 cases) or pituitary tumours (14 cases). This suggests some challenges in distinguishing gliomas from other tumour types, particularly meningiomas. Meningiomas proved the most challenging for the model, with 218 correct identifications out of 306 cases (71.2% recall). The model showed difficulty distinguishing meningiomas from other classes, misclassifying 58 as pituitary tumours, 20 as gliomas, and 10 as non-tumorous. This aligns with the lower accuracy for meningiomas, indicating an area where the model could benefit from further refinement. Interestingly, the model rarely misclassified tumours as non-tumorous (only 10 meningioma cases), indicating a low false negative rate for tumour detection overall. This is crucial for a diagnostic aid tool, as missing tumours would be more problematic than occasional false positives. The relatively low Recall and F1-score recorded for the meningioma class can further be improved by tuning the decision threshold to favor true positives. For classification models, lowering the decision threshold can increase recall by classifying more instances as positive, even at the risk of increased false positives.

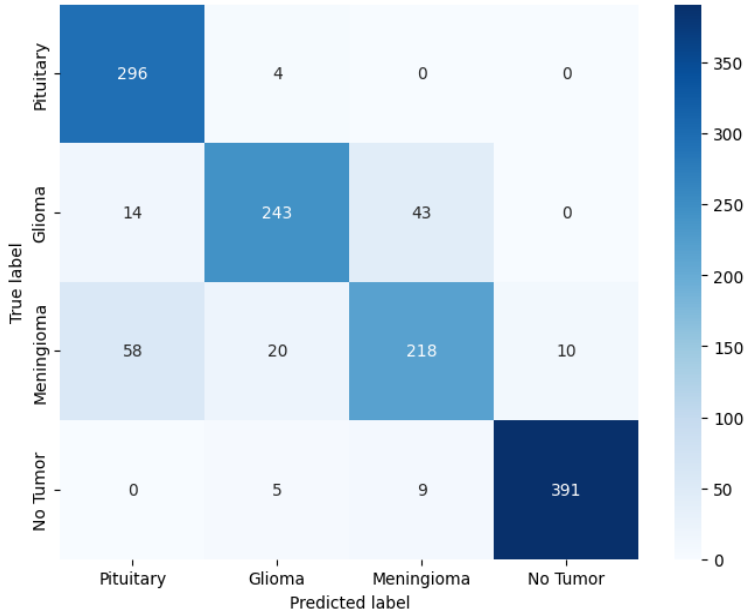

Fig. 10. Confusion matrix of the classification model.

Fig. 11 shows the ROC curve of the classification model. The results demonstrate the model's exceptional ability to differentiate between four brain tumour categories: Pituitary, Glioma, Meningioma, and No tumour. The model achieves near-perfect classification for No tumour (AUC = 1.00) and exhibits very high accuracy for Pituitary (AUC = 0.99) and Glioma (AUC = 0.98). While still performing well, the model shows slightly lower accuracy for Meningioma (AUC = 0.95). These results highlight the model's potential as a valuable tool for accurate brain tumour classification, aiding in diagnosis and treatment planning.

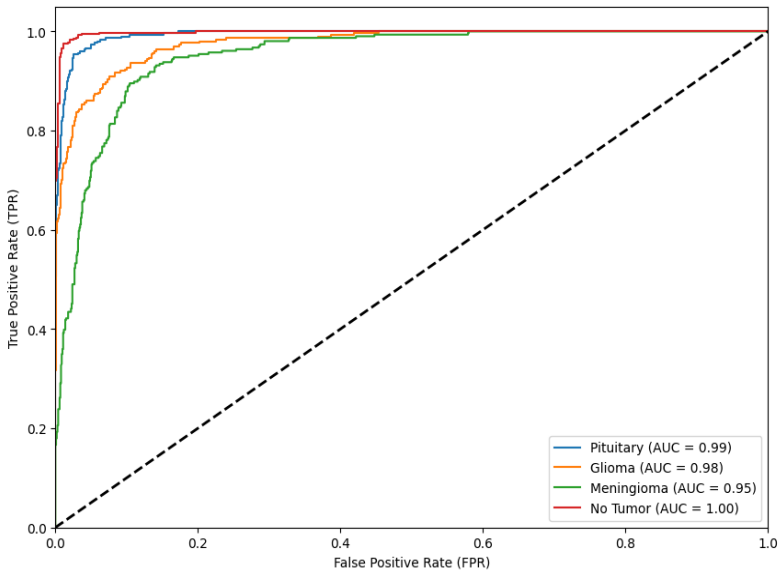

Fig. 11. ROC curve for each class of the classification model.

4.3 Compared Performance Analysis

The performance of the developed model was compared with established state-of-the-art methods in brain tumour segmentation and classification. The results demonstrate competitive performance across key metrics.

4.3.1 Tumour Detection and Segmentation

Table 6 shows the comparison of the developed model with existing studies under the detection accuracy category. As can be observed in Table 5, the developed model in this study outperformed other studies in terms of the Dice coefficient and IoU score respectively. In all these studies [23-25], only one of the metric was used to evaluate the model performance. In the current study, both the Dice coefficient and IoU score were used to provide robust performance analysis.

Table 6. Comparison of brain tumour detection models.

Study	Model Used	Dice Coefficient	IOU Score
[23]	DeepMedic (3D CNN)	0.89	-
[24]	3D U-Net	-	0.723
[25]	Ensemble CNN	0.8839	-
Current Study	U-Net	0.9321	0.8729

4.3.2 Tumour Classification

Table 7 presents the comparison of the developed model with other related studies for brain tumour classification. As shown in Table 6, the EfficientNet-based model achieved an overall accuracy of 0.965, with class-specific F1-scores ranging from 0.76 (meningioma) to 0.97 (no tumour). The proposed methodology aligns well with the current state-of-the-art in brain tumour analysis, demonstrating competitive performance in both segmentation and classification tasks.

Table 7. Comparison of brain tumour classification models.

Study	Model Used	Accuracy
[26]	Capsule Network	0.909
[27]	VGG-19	0.875
[28]	CNN with Gaussian Noise	0.9464
[29]	CNN with NN classifier	0.9586
[30]	CNN with enhanced classifiers	0.96
[31]	Federated learning	0.9105
[32]	VGG-16 with integration of CNN	0.9374
Current Study	EfficentNet	0.965

4.4 Result from Web Interface

The final look of the web interface and the model test with sample images are shown in Fig. 12 and Fig. 13. Figure 12 displays the landing page of the brain tumour detection web interface and it features a brief description of the tool's capabilities, and instructions for uploading MRI images. Fig. 13 demonstrates the results page with analysed MRI images and user feedback. It shows the analysis of two MRI images, with one identified as having a glioma tumour and the other showing no abnormalities.

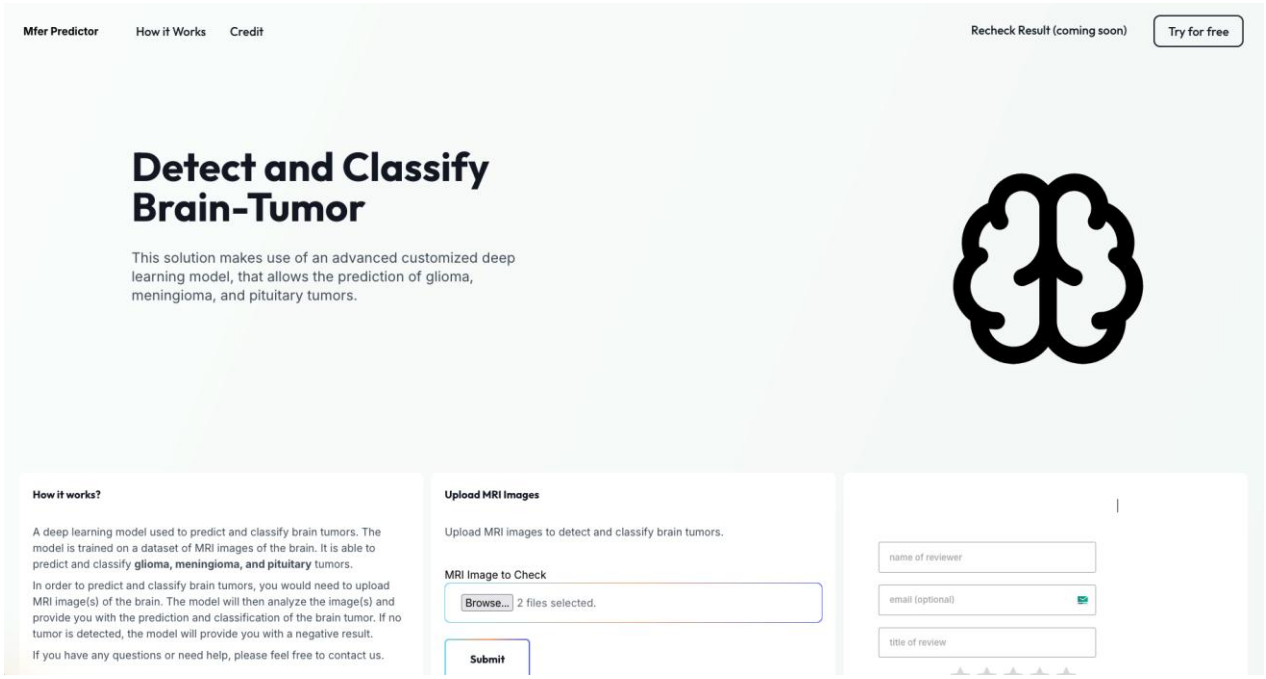

Fig. 12. Landing page of the web interface.

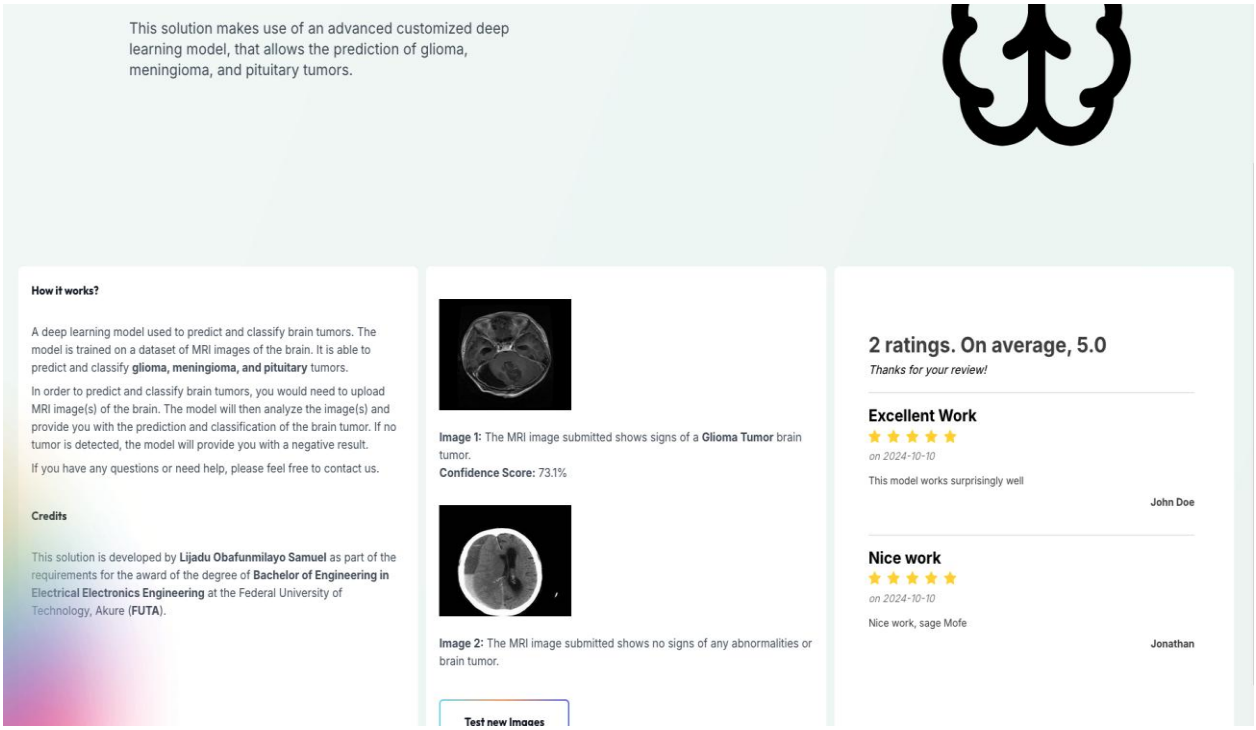

Fig. 13. Sample MRI image analysis results from the models.

5. Conclusion

Deep learning techniques have emerged as powerful tools in the field of medical image analysis, particularly in the domain of brain tumour detection and classification. This study has explored the application of advanced neural network architectures to address the critical challenge of accurately identifying and categorising brain tumours from MRI scans. This study uses an integration of convolutional neural networks, specifically U-Net for segmentation and EfficientNet for classification. These models have demonstrated the potential of deep learning to enhance the accuracy and efficiency of brain tumour diagnosis. These models have shown capability in capturing complex patterns and features in medical images that may not be immediately apparent to the human eye. The results presented show that the developed models have superior performance over other related studies. The detection model achieves a Dice coefficient of 0.9321 and an IoU score of 0.8729, while the classification model attains an overall accuracy of 0.965. In addition, a user-friendly web interface was developed to enhance the system's practicality for clinical use. In order to improve the accuracy of tumour identification, segmentation, and classification in comparison to single-modality images, future research will examine a multi-modal integration for brain tumour detection that integrates data from various MRI sequences (such as T1-weighted, T2-weighted, and FLAIR) and CT scans to provide complementary morphological and pathological information.

References

[1] R. Kaifi. “A review of recent advances in brain tumour diagnosis based on AI-Based classification,” *Diagnostics*, 2023, vol. 13, no. 18, pp. 1-32.
[2] J. Amin, M. Sharif, M. Yasmin, and S.L. Fernandes. “A distinctive approach in brain tumor detection and classification using MRI,” *Pattern Recognition Letters*, 2020, vol. 139, pp. 118-127.
[3] F. Fahmi, F. Apriyulida, I.K. Nasution, and Sawaluddin. “Automatic detection of brain tumor on computed tomography images for patients in the intensive care unit,” *Journal of Healthcare Engineering*, 2020, vol. 1, pp. 1-13.
[4] T.Z. Wong, G.J. van der Westhuizen, and R.E. Coleman. “Positron emission tomography imaging of brain tumors,” *Neuroimaging Clinics*, 2002, vol. 12, no. 4, pp. 615-626.
[5] S.M. Stufflebeam, N. Tanaka, and S.P. Ahlfors. “Clinical applications of magnetoencephalography,” *Human Brain Mapping*, 2009, vol. 30, no. 6, pp. 1813-1823.
[6] M. Nazir, S. Shakil, and K. Khurshid. “Role of deep learning in brain tumour detection and classification (2015 to 2020): A review,” *Computerised Medical Imaging and Graphics*, 2021, vol. 91, p.101940.
[7] N. Abiwinanda, M. Hanif, S.T. Hesaputra, A. Handayani, and T.R. Mengko. “Brain tumour classification using convolutional neural networks,” In *IFMBE Proceedings*, 2018, 183–189.
[8] A. Ari, and D. Hanbay. “Deep learning based brain tumour classification and detection system,” *Turkish Journal of Electrical Engineering and Computer Sciences/Elektrik*, 2018, vol. 26, no. 5, pp. 2275–2286.

[9] S. Das, O.F. Aranya, and N.N. Labiba. "Brain tumour classification using convolutional neural networks," *In Proceedings of the 1st International Conference on Advances in Science, Engineering and Robotics Technology*, 3-5 May 2019, Dhaka, Bangladesh.
[10] S. Deepak, and P. Ameer, "Brain tumour classification using deep CNN features via transfer learning," *Computers in Biology and Medicine*, 2019, vol. 111, p. 103345.
[11] S. Manjunath, M.B. Sanjay Pande, B.N. Raveesh, and G.K. Madhusudhan. "Brain tumour detection and classification using convolutional neural network," *In Proceedings of the Second International Conference on Emerging Trends in Science and Technologies for Engineering Systems*, 17-18 May 2019, Karnataka, India.
[12] S. Sajid, S. Hussain, and A. Sarwar. "Brain tumour detection and segmentation in MR images using deep learning," *Arabian Journal for Science and Engineering*, 2019, vol. 44, no. 11, pp. 9249–9261.
[13] W. Ayadi, W. Elhamzi, I. Charfi, and M. Atri,. "Deep CNN for brain tumour classification," *Neural Processing Letters/Neural Processing Letters*, 2021, vol. 53, no. 1, pp. 671–700.
[14] A. Çinar, and M. Yildirim. "Detection of tumours on brain MRI images using the hybrid convolutional neural network architecture," *Medical Hypotheses*, 2020, vol. 139, p. 109684.
[15] R. Hashemzehi, S.J.S. Mahdavi, M. Kheirabadi, and S.R. Kamel. "Detection of brain tumours from MRI images based on deep learning using hybrid models CNN and NADE," *Biocybernetics and Biomedical Engineering*, 2020, vol. 40, no. 3, 1225–1232.
[16] S.A. Ismael, A. Mohammed, and H. Hefny. "An enhanced deep learning approach for brain cancer MRI images classification using residual networks," *Artificial Intelligence in Medicine*, 2020, vol. 102, p. 101779.
[17] T. Saba, A.S. Mohamed, M. El-Affendi, J. Amin, and M. Sharif. "Brain tumour detection using fusion of hand crafted and deep learning features," *Cognitive Systems Research*, 2020, vol. 59, pp. 221–230.
[18] M.I. Sharif, J.P. Li, M.A. Khan, and M.A. Saleem. "Active deep neural network features selection for segmentation and recognition of brain tumours using MRI images," *Pattern Recognition Letters*, 2020, vol. 129, pp. 181–189.
[19] J. Amin, M. Sharif, M. Yasmin, and S.L. Fernandes. "A distinctive approach in brain tumour detection and classification using MRI," *Pattern Recognition Letters*, 2020, vol. 139, pp. 118–127.
[20] T. Sadad, A. Rehman, A. Munir, T. Saba, U. Tariq, N. Ayesha, and R. Abbasi. "Brain tumour detection and multi-classification using advanced deep learning techniques," *Microscopy Research and Technique*, vol. 84, no. 6, pp. 1296–1308.
[21] F. Turk, and M. Kılıçaslan. "Lung image segmentation with improved U-Net, V-Net and Seg-Net techniques," *PeerJ Computer Science*, 2025, vol. 11, pp. 1-21.
[22] J. Jayapradha, S.C. Haw, N. Palanichamy, S.K. Thillaigovindhan, and M. Al-Tarawneh. "Lung tumor segmentation in medical imaging using U-NET," *Journal of Informatics and Web Engineering*, 2025, vol. 4, no. 1, pp. 140-151.
[23] K. Kamnitsas, C. Ledig, V.F. Newcombe, J.P. Simpson, A.D. Kane, D.K. Menon, D. Rueckert, and B. Glocker. "Efficient multi-scale 3D CNN with fully connected CRF for accurate brain lesion segmentation," *Medical Image Analysis*, 2016, vol. 36, pp. 61-67.
[24] Ö., Çi çek, A. Abdulkadir, S.S. Lienkamp, T. Brox, and O. Ronneberger. "3D U-Net: Learning dense volumetric segmentation from sparse annotation," In *Lecture Notes in Computer Science*, 2026, pp. 424-432.
[25] A. Myronenko. "3D MRI brain tumour segmentation using autoencoder regularisation. In: A. Crim, S. Bakas, H. Kuijf, F. Keyvan, M. Reyes and T. van Walsum (eds.) Brainlesion: Glicoma, Multiple Sclerosis, Stroke and Traumatic Brain Injury. *Lecture notes in Computer Science*, 2018, vol. 11384, 311-320, Springer.
[26] P. Afshar, A. Mohammadi, and K.N. Plataniotis. "Brain tumour type classification via capsule networks," In: Proceedings of the *26th IEEE International Conference on Image Processing*, 22-25 September 2019, Taipei, Taiwan, 1570-1574.
[27] M. Sajjad, S. Khan, K. Muhammad, W. Wu, A. Ullah, and S.W. Baik, "Multi-grade brain tumour classification using deep CNN with extensive data augmentation," *Journal of Computational Science*, 2019, vol. 30, pp. 174-182.
[28] L. Gaur, M. Bhandari, T. Razdan, S. Mallik, and Z. Zhao, "Explanation-driven deep learning model for prediction of brain tumour status using MRI image data," *Frontiers in Genetics*, 2022, vol. 13, p.822666.
[29] A. Vidyarthi, R. Agarwal, D. Gupta, R. Sharma, D. Draheim, and P. Tiwari, "Machine learning assisted methodology for multiclass classification of malignant brain tumors," *IEEe Access*, 2022, vol. 10, pp.50624-50640.
[30] D. Lamrani, B. Cherradi, O. El Gannour, M.A. Bouqentar, and L. Bahatti, "Brain tumor detection using MRI images and convolutional neural network," *International Journal of Advanced Computer Science and Applications*, 2022, vol. 13.
[31] M. Islam, M.T. Reza, M. Kaosar, and M.Z. Parvez, "Effectiveness of federated learning and CNN ensemble architectures for identifying brain tumors using MRI images," *Neural Processing Letters*, 2023, vol. 55, pp.3779-3809.
[32] A. Alshammari, "Construction of VGG16 convolution neural network (VGG16 CNN) classifier with NestNet-based segmentation paradigm for brain metastasis classification," *Sensors*, 2022, vol. 22, pp. 1-19.

Authors' Profiles

Kazeem B. Adedeji received his B.Eng and M.Eng. degrees in Electrical and Electronics Engineering from Federal University of Technology Akure (FUTA), and M.Tech. and PhD degrees in Electrical Engineering from Tshwane University of Technology, Pretoria, South Africa. He was involved in research collaborations with colleagues at FUTA and other universities such as Tshwane University of Technology, Pretoria and University of Johannesburg. He has several publications in peer reviewed international journals. His research interests span the areas of wireless sensor networks, communication security, biomedical image analysis, AI and electromagnetic compatibility.

Obafunmilayo Lijadu recently graduated with a Bachelor of Engineering (B.Eng) in Electrical and Electronics Engineering. His primary research interest encompasses machine learning and control engineering, with a particular focus on the application of deep learning algorithms for medical image analysis.

Wasiu Lawal, PhD Communication Engineering, and a member of the Department of Information and Communication Engineering under the School of Electrical Systems Engineering (SESE), The Federal University of Technology, Akure (FUTA), Ondo State, Nigeria. His areas of scientific interest include the development of intelligent models for robust signal detection and estimation, with applications in Artificial Intelligence and Machine Learning (ML).

How to cite this paper: Kazeem B. Adedeji, Obafunmilayo S. Lijadu, Wasiu Lawal, "Development of a Brain Tumour Detection and Classification Model with Web Application Capability", International Journal of Engineering and Manufacturing (IJEM), Vol.15, No.6, pp. 1-15, 2025. DOI:10.5815/ijem.2025.06.01